Surface-Modified Melt Coextruded Nanofibers Enhance Blood Clotting In Vitro

Justin D. Hochberg, David M. Wirth, and Jonathan K. Pokorski*

Blood loss causes an estimated 1.9 million deaths per year globally, making new methods to stop bleeding and promote clot formation immediately following injury paramount. The fabrication of functional hemostatic materials has the potential to save countless lives by limiting bleeding and promoting clot formation following an injury. This work describes the melt manufacturing of poly(ϵ -caprolactone) nanofibers and their chemical functionalization to produce highly scalable materials with enhanced blood clotting properties. The nanofibers are manufactured using a high throughput melt coextrusion method. Once isolated, the nanofibers are functionalized with polymers that promote blood clotting through surface-initiated atom transfer radical polymerization. The functional nanofibers described herein speed up the coagulation cascade and produce more robust blood clots, allowing for the potential use of these functional nonwoven mats as advanced bandages.

1. Introduction

Functional polymeric nanofibers have attracted significant attention in recent years due to their vast applications in biomedicine. Some of these applications include drug delivery (where fibrous materials can provide low diffusion distances), tissue engineering (where the high surface area to volume ratio leads to high porosity and ample sites for cellular adhesion), and wound intervention (where altering the surface characteristics of nanofibers can lead to excellent antibacterial effectiveness without compromising biocompatibility). [1-6] The need for improving human health has been instrumental in leading advances in polymer processing technology and surface modification chemistries, which have helped usher in a new generation of functional biomaterials.

The literature describes a multitude of nanofiber fabrication methods, each with associated advantages and challenges. The most common method for fiber fabrication is electrospinning due to its simple and inexpensive setup, and the ability to control the dimensions of the fabricated fibers down to the nanoscale. [4,7] Electrospinning is useful in a variety of research applications;

J. D. Hochberg, D. M. Wirth, J. K. Pokorski Department of NanoEngineering, Jacobs School of Engineering University of California San Diego La Jolla, CA 92093, USA E-mail: jpokorski@eng.ucsd.edu

The ORCID identification number(s) for the author(s) of this article can be found under https://doi.org/10.1002/mabi.202200292

DOI: 10.1002/mabi.202200292

however, the quality and size of fibers produced are highly dependent on the processing parameters of the system.[8,9] Additionally, electrospinning has a low maximum throughput, 200 g h⁻¹, which may limit the commercial translation of this method.[10] Researchers have since developed new nanofiber manufacturing techniques, but these also present limitations: fibers made via rotary jet spinning exhibit weak mechanical properties,[11,12] melt blowing is a challenging method to produce fibers with dimensions in the nanoscale,[13] and melt electrospinning requires high voltages while providing a throughput that is lower than traditional electrospinning.[14] To combat these issues, melt coextrusion has recently emerged as a nanofiber fabrication method that is scalable, solvent-free,

and yields nanoscale fibers. [15] Melt coextrusion provides the ability to create fibers with easily tunable cross-sectional dimensions and mechanical properties. The manufacturing process is solvent-free and continuous, producing material at a rate of 2 kg h $^{-1}$, significantly outperforming comparable electrospinning methods. [15–17] Recent work has utilized these materials for various applications including for use as fuel filters, [18] biomedical scaffolds, [17,19] and as antibacterial materials to name a few. [5]

Fibers fabricated via melt coextrusion can be produced from most extrudable thermoplastic polymers, but have certain requirements when used in the biomedical arena.[4,20] First and foremost, nanofibers intended for biomedical applications must be biocompatible. Other advantageous characteristics include having favorable degradation kinetics, mechanical properties, and the ability to introduce chemical or biochemical modifications.^[4] Effective biomaterial scaffolds cannot be cytotoxic nor should they induce or suppress the immune system in an undesirable manner.[21] A common class of materials used in biomedical applications are polyesters as they are well established to be non-cytotoxic and have a long history of use in FDA-approved devices.^[22] Commonly utilized polyesters include poly(lactic acid) (PLA), poly(glycolic acid) (PGA), and poly(ϵ caprolactone) (PCL). PCL in particular is known for its flexibility (reaching more than 700% elongation at break)[16] and its slow hydrolytic degradation rate (2-3 years).[23,24]

Unmodified polyester nanofibers do not possess functional biologically active properties that would improve their utility in most biomedical applications, such as tissue engineering or wound treatment.^[5,25] Properties that may improve biomedical outcomes can be enhanced by introducing bio-active

www.advancedsciencenews.com



rials with varying properties, as well as the ability to incorporate other relevant functionalities. Melt-extruded nanofibers are ideal hemostatic surfaces due to their ability to be fabricated at large scale and their intrinsic high surface area which would put even large wounds in contact with high surface functionality for contact-based hemostasis. We anticipate that this would be preferable to the tissue factor mediated coagulation scheme due to high costs associated with producing large amounts of clotting factors, difficulty in long-term storage at sites that would be in need of large scale wound dressings (e.g. the military arena), and challenges in integrating tissue factors into materials. [42,43,46] We describe the fabrication of melt coextruded PCL nanofiber mats and their subsequent functionalization utilizing a graftingfrom surface-initiated atom transfer radical polymerization (SI-ATRP), due to its high grafting efficiency and ease of fiber modification. The surfaces are modified to control their hydrophobic/hydrophilic balances, leading to an enhancement of the rate and robustness of blood clotting.[43]

moieties onto the surface of the nanofiber. There are many potential functionalization methods of polyesters including end group modification, [26] hydrolysis, [27] aminolysis, [28] and photochemical covalent modification. [29] Chemical modification of nanofiber scaffolds has allowed for the fabrication of antifouling [30] and antibacterial mats, [5] as well as the creation of platforms for cellular adhesion, growth, proliferation, and differentiation mimicking the extracellular matrix (ECM). [7,17,20]

Functional nanofibers offer unique solutions for wound treatment due to their high porosity and large surface area. Their use as hemostatic materials provides a simple solution to hemorrhagic trauma. Hemorrhagic shock is a condition of extreme blood loss which leads to inadequate oxygen delivery to organs and tissues. Each year, 60,000 deaths in the United States and 1.9 million deaths worldwide occur from hemorrhaging.[31,32] Following any vascular injury resulting in escaping blood, the body's aim is to prevent further blood loss by "plugging the hole." This is done via the gelation of blood by activating a thrombin-mediated coagulation cascade. Through a series of enzyme-mediated reactions, a fibrin mesh is formed at the site of injury, resulting in a stable clot.[33-39] There are two main mechanisms that induce the coagulation cascade, first is the extrinsic or tissue factor (TF) pathway, which occurs in traditional hemostasis when cells that are expressing a tissue factor protein encounter blood plasma, triggering the clotting cascade. The second method of initiating the coagulation cascade is via the intrinsic or contact pathway. The contact pathway occurs when plasma encounters specific types of artificial surfaces such as diatomaceous earth, glass, or clay amongst others. Blood contact with one of these surfaces causes a plasma protein, factor XII, to change conformation, thus activating the coagulation cascade. This pathway does not contribute to natural hemostasis, but does participate in thrombotic diseases.[40,41]

Utilizing the contact pathway unlocks the potential to modify the surface of a material to trigger a desired clotting event. Sperling and colleagues studied the effects of varying hydrophobicity and its impact on blood clotting. Experiments with varying ratios of alkyl (-CH₃) and carboxylic acid (-COOH) groups on glass surfaces were tested and it was concluded that neither solely alkyl nor carboxylic acid were the ideal surface to promote blood clotting. Alkyl surfaces displayed the largest numbers of adherent platelets, while carboxylic acid surfaces had the greatest contact activation. However, neither showed superior clotting abilities when compared with a surface comprised of both functional groups. Superior clotting required a balancing act between contact activation and platelet adhesion, and that balance had a strong synergistic effect on the successfulness and degree of blood clotting. [42] Further studies have expanded on this, varying the length of alkyl chains present, showing that the most effective surface coating was a random co-polymer with a ratio of 65% acrylic acid (AA) to 35% butyl methacrylate (BMA).[43]

This manuscript describes the fabrication of functional nanofiber mats that improve blood clotting to quickly form more robust clots. Current hemostatic wound treatment devices typically feature either an artificially formed blood clot^[44] or materials made specifically of a hemostatic agent such as chitosan.^[45] Therefore, these materials are limited in the material properties that can be bestowed on the devices. Creating functional nanofiber mats allows for the use of a wide variety of mate-

2. Results and Discussion

2.1. Fabrication of Melt Coextruded Nanofiber Mats

PCL nanofibers were prepared via a melt coextrusion process, as previously described. Poly(ethylene oxide) (PEO) was used as an coextrudate due to its immiscibility with PCL leading to well defined layer separation and easy delamination through aqueous dissolution.^[5] Melt coextrusion proceeded by individually pumping PEO and PCL into the extrusion line, where each polymer was stacked on top of one another. A 90° rotation immediately followed this process wherein the two melt flows were oriented side by side (**Figure 1**A). The melt was then sent through an "n" number of vertical multipliers (n = 16), where each multiplier doubled the amount of vertical layers. This series of multiplication steps created 2^{n+1} vertical layers (Figure 1B). A 33% by volume PEO skin layer was then pumped on top and bottom of the melt flow (Figure 1C). Finally, the melt was passed through a series of "m" number of horizontal multipliers, establishing 2^m (m= 4) horizontal layers and 2^{n-m} vertical layers (Figure 1D), resulting in 4096 × 116 PCL domains embedded in a PEO matrix.

The resulting extrudate is a composite material with PCL fibers embedded within a sacrificial PEO matrix. PCL nanofiber scaffolds were obtained by removal of the hydrophilic PEO matrix. The composite tapes were washed in an agitated water bath to remove the bulk of the PEO phase. Following the initial washing, the water is replaced with a 70% MeOH bath and left overnight to remove the majority of the PEO. Finally, the nanofibers are treated with a high-pressure water jet to 1) entangle the nanofibers to create non-woven mats and to 2) remove any remaining PEO which is difficult to completely remove with just a water/MeOH bath. This process removes 97% of the PEO from the nanofibers (Figure S1, Supporting Information).^[5] Circular segments were punched out of the resulting nanofiber sheets (6 mm) to facilitate well-plate assays.

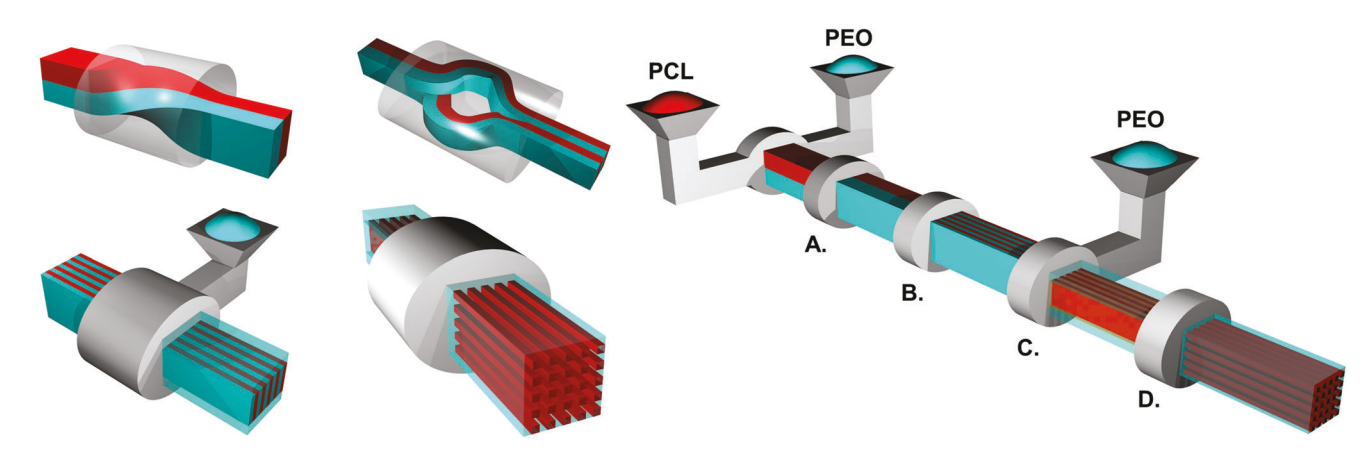
2.2. Nanofiber Functionalization with Photochemistry and SI-ATRP

Grafting functional polymers off of the nanofiber surface first required the covalent conjugation of an atom transfer radical

16165195, 0, Downloaded from https://onlinelibrary.wiley.com/doi/10.1002/mabi.202200292 by University Of California, Wiley Online Library on [13/10/2022]. See the Terms and Conditions (https://onlinelibrary.wiley.com/term

s-and-conditions) on Wiley Online Library for rules of use; OA articles are governed by the applicable Creative Commons License

A. Layer Rotation B. Vertical Multiplication



C. Surface Layering D. Horizontal Multiplication

Figure 1. Schematic diagram of melt coextrusion utilizing A) layer rotation, B) vertical multiplication, C) surface layering, and D) horizontal multiplication procedures.

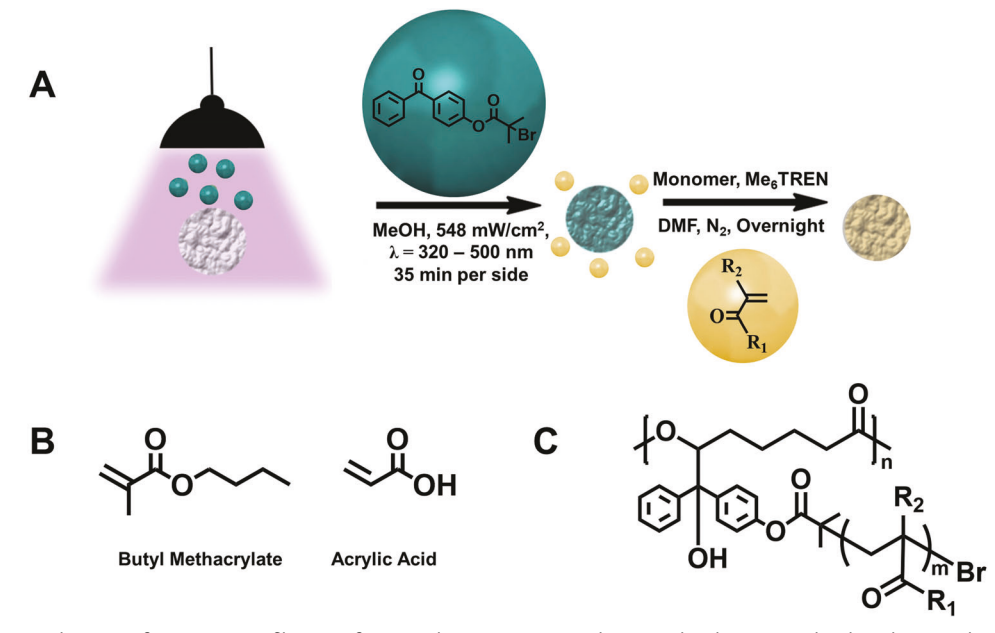


Figure 2. A) Schematic diagram of SI-ATRP nanofiber mat functionalization. Mats are dip-coated with initiator, dried, and exposed to UV light. This is followed by standard ATRP conditions. B) Chemical structure of monomers used in nanofiber mat functionalization. C) Chemical structure of functionalized nanofibers.

polymerization (ATRP) initiator onto the fiber.^[5] Benzophenone modified with a tertiary bromide was first synthesized to act as an ATRP initiator. This molecule is known to undergo photochemical hydrogen abstraction, followed by radical insertion into the PCL backbone, yielding a tertiary bromide functionalized nanofiber surface.^[29,47] Nanofiber mats were dip-coated in a solution containing the benzophenone-ATRP initiator and allowed to dry to create a coating on the surface. Dried and coated mats were subsequently exposed to UV light to initiate the photochem-

ical transformation, yielding bromide functionalized mats ready to undergo SI-ATRP.

SI-ATRP was conducted from the modified nanofiber surface to alter the hydrophobic/hydrophilic balance (Figure 2A). Studies comparing the roles of carboxylic acid and alkyl functionalities have shown that differing ratios of the two have a significant impact on the formation and quality of blood clots. The ideal composition was a statistical copolymer of 65% AA and 35% BMA (Figure 2B), which significantly improved the rate and

16165195, Downloaded from https://onlinelibrary.wiley.com/doi/10.1002/mabi.20220029 by University Of California, Wiley Online Library on [1310/2022]. See the Terms and Conditions (https://onlinelibrary.wiley.com/terms-and-conditions) on Wiley Online Library for rules of use; OA articles are governed by the applicable Creative Commons Licenses

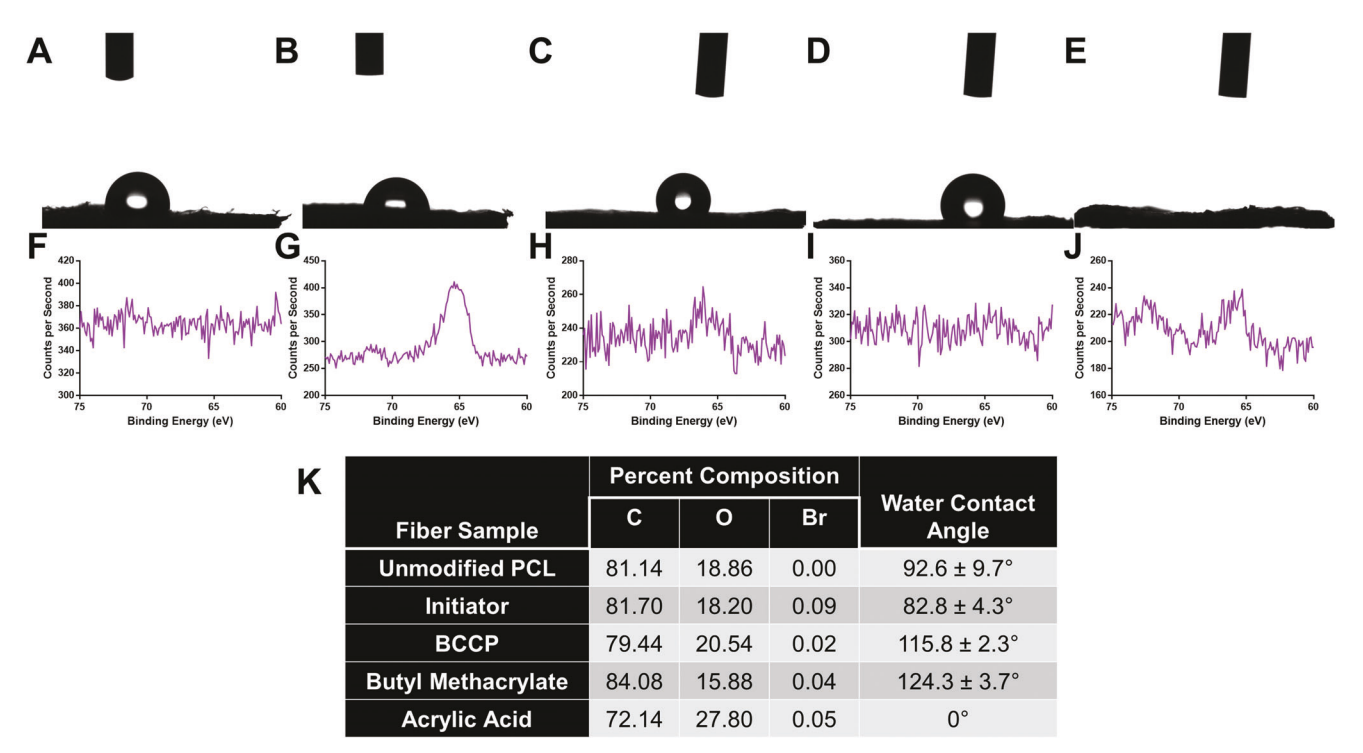


Figure 3. Surface characterization of functionalized nanofiber mats. WCA measurements of A) PCL, B) initiator, C) BCCP, D) butyl methacrylate, and E) acrylic acid functionalized nanofiber mats. High-resolution XPS spectra of Br 3d on F) PCL, G) initiator, H) BCCP, I) butyl methacrylate, and J) acrylic acid functionalized nanofiber mats. K) Table summarizing XPS and WCA results.

quality of fibrin blood clots as compared with other variations and controls.^[43] We compared this composition with surfaces functionalized with acrylic acid, butyl methacrylate, and unmodified PCL (Figure 2C). Functionalization was first confirmed with water contact angle (WCA), which is used to show differences in the surface energy of a material, allowing for the determination of chemically distinct surfaces. As the hydrophilicity of a material's surface increases, the contact angle approaches 0; and as hydrophobicity increases the value of the contact angle trends oppositely. In general, a WCA greater than 90° is considered hydrophobic and less than 90° is considered hydrophilic.^[48] Upon functionalization of the PCL fibers with the ATRP initiator, the WCA decreases slightly from 92.6 \pm 9.7° (Figure 3A) to 82.8 \pm 4.3° (Figure 3B), indicating that the ATRP initiator may make the sample more hydrophilic. The water contact angle of the blood clotting copolymer (BCCP), increased to $115.8 \pm 2.3^{\circ}$ (Figure 3C) indicating that the hydrophobic effects of the exposed hydrocarbon tail of BMA dominate the surface energy relative to the hydrophilic effects of the carboxylic acid from AA. Our control fiber mats used either a BMA homopolymer displaying a WCA of 124.3 \pm 3.7° (Figure 3D), or an AA homopolymer showing a WCA of 0° (Figure 3E), indicating complete wetting.

X-ray photoelectron spectroscopy (XPS) was used to further characterize the modified fiber mats by providing information about the chemical composition of the nanofiber surface. Quantifiable variations in atomic surface composition confirm the successful functionalization of the material. High-resolution spectra show the successful incorporation of bromine in the initiator and polymer functionalized nanofibers, due to the presence of bromine in the benzophenone ATRP initiator and end groups of

the respective polymers (Figure 3F–J). Survey spectra confirm the lack of any unanticipated elements present in the samples (Figure S2A-E, Supporting Information). Figure 3K summarizes the quantitative data from the WCA and XPS plots and shows that incorporating solely BMA increases the carbon:oxygen ratio while incorporating only AA significantly decreases the carbon:oxygen ratio. The ratio of BCCP-modified surfaces is between the carbon:oxygen ratios of the BMA and AA modified mats and verifies the copolymerization of both monomers and approximates that anticipated 65/35% ratio. Analysis of the XPS results utilizing peak integration reveals a composition of $61.0 \pm 0.02\%$ acrylic acid and $39.0 \pm 0.02\%$ butyl methacrylate, close to the desired ratio of 65%/35%. Scanning electron micrographs confirm that the functionalization does not have any meaningful impact on nanofiber morphology when comparing the functionalized nanofibers (Figure 4A-C,E-G) with unmodified PCL (Figure 4D,H).

2.3. In Vitro Blood Clotting Experiments

2.3.1. Plasma Recalcification Time

Plasma recalcification time (PRT) is a qualitative study determining the length of time it takes a clot to form. Ca²⁺ ions have been known since the late 1800s to be an essential part of the blood coagulation cascade,^[49] and blood products are commonly inactivated with anticoagulants such as sodium citrate to stabilize and preserve them.^[50] PRT studies reintroduce a calcium source, and measure the time until a gel forms, indicating the formation of a fibrin clot (**Figure 5**A,B). Citrated plasma was incubated

16165195, 0, Downloaded from https://onlinelibrary.wiley.com/doi/10.1002/mabi.202200292 by University Of California, Wiley Online Library on [13/10/2022]. See the Terms and Conditions (https://onlinelibrary.wiley.com/term

-and-conditions) on Wiley Online Library for rules of use; OA articles are governed by the applicable Creative Commons License

Figure 4. Scanning electron micrograph of nanofiber mats of BCCP (A,E), butyl methacrylate (B,F), acrylic acid (C,G), and unmodified PCL (D,H) nanofiber mats. Scale bars indicate 50 μm (A–D) and 5 μm (E–H).

with CaCl₂ and nanofiber mats. The time was recorded once the plasma solution became cloudy and would adhere to the mat indicating the transformation from a liquid to a solidified gel. Control samples included clots formed in well plates without a fiber mat and clots formed on unmodified PCL mats, which dis-

played similar PRTs of 215.5 ± 6.4 and 210.0 ± 1.4 s, respectively. BCCP and BMA modified fiber mats significantly decreased the PRT with values of 183.5 ± 9.2 and 191.4 ± 4.2 s, respectively, indicating both materials accelerated the blood clotting process. AA modified mats significantly increased the amount of time it

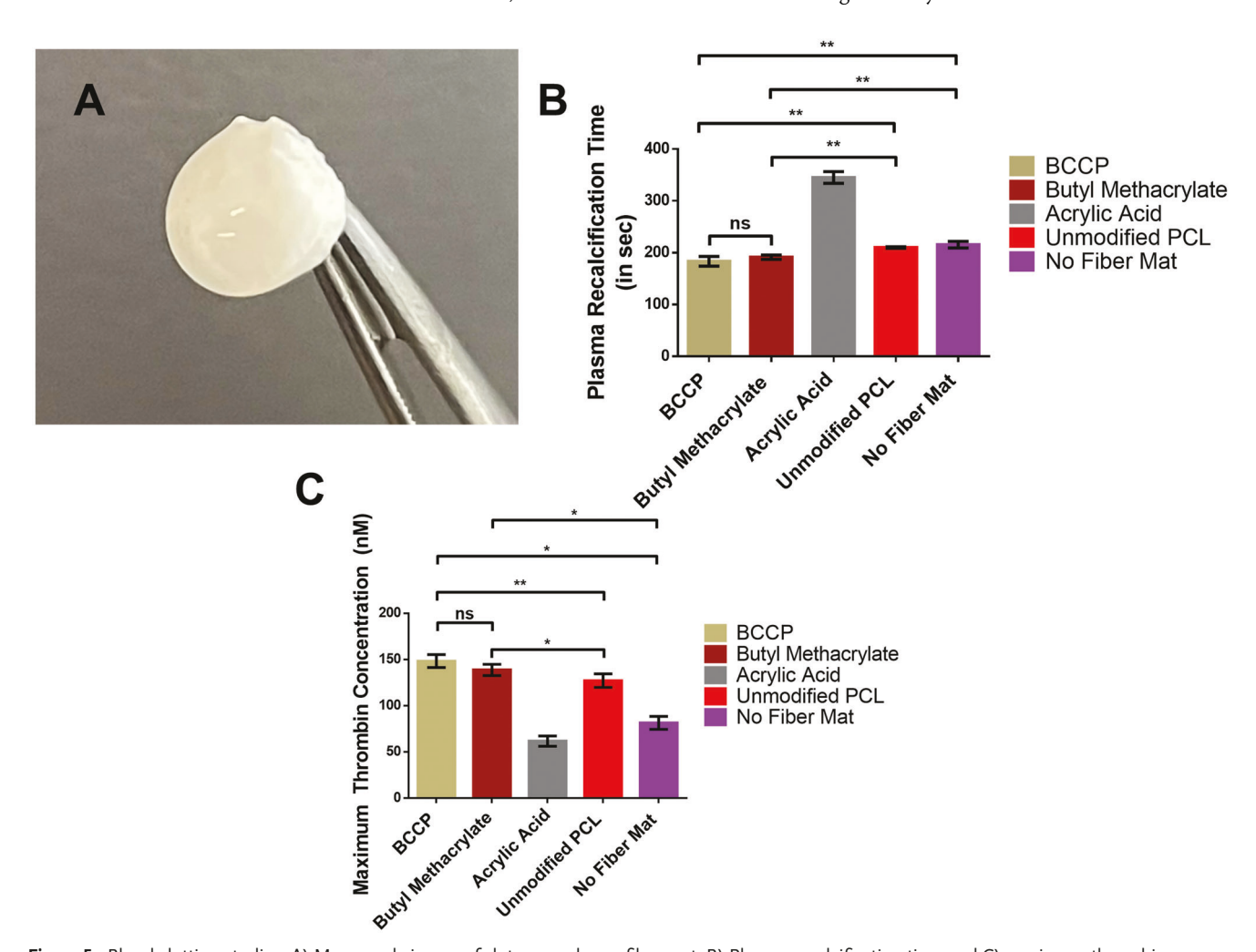


Figure 5. Blood clotting studies. A) Macroscale image of clot covered nanofiber mat. B) Plasma recalcification time and C) maximum thrombin concentrations from thrombin generation assay plots of the various clots. * $p \le 0.05$ and ** $p \le 0.01$.

16165195, Downloaded from https://onlinelbrary.wiley.com/doi/10.1002/mabi.202200292 by University Of California, Wiley Online Library on [13/10/2022]. See the Terms and Conditions (https://onlinelbbrary.wiley.com/terms-and-conditions) on Wiley Online Library for rules of use; OA articles are governed by the applicable Creative Commons Licenses

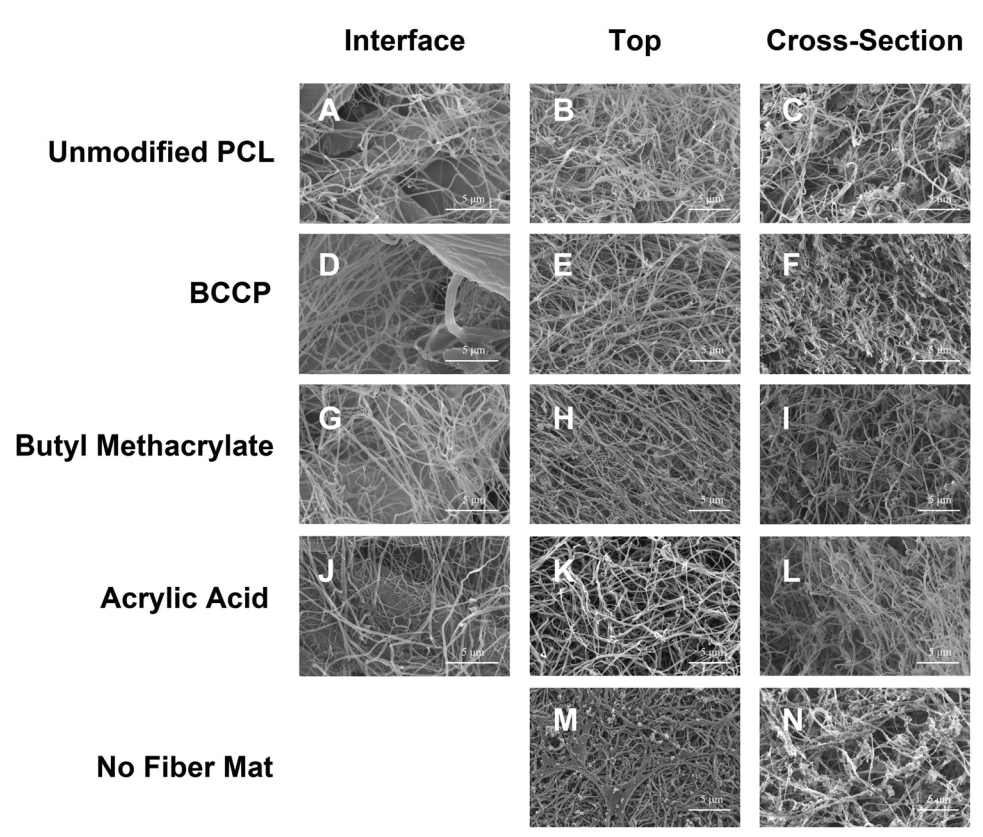


Figure 6. A–N) Scanning electron micrograph of nanofiber mats of PCL (A–C), BCCP (D–F), butyl methacrylate (G–I), acrylic acid (J–L), and no nanofiber mat present (M,N). Images include clot-nanofiber interface (A,D,G,J), top of clots (B,E,H,K,M), and clot cross-sections (C,F,I,L,N). Scale bars indicate 5

took for plasma recalcification to 345.1 ± 11.3 s, indicating that anticoagulation properties in mats modified with just acrylic acid.

2.3.2. Thrombin Generation Assay

A key step of the blood coagulation cascade and the formation of a blood clot is the thrombin-mediated conversion of fibrinogen to fibrin. Thrombin concentrations are directly correlated with the strength and stability of fibrin fibers, with high concentrations producing thicker, more dense networks of highly branched fibrin fibers, which are resistant to fibrinolysis. [37,39,51] A thrombin generation assay (TGA) was conducted to determine the maximum thrombin concentrations (MTC) of the functional nanofiber mats and controls (Figure 5C and Figure S3, Supporting Information). BCCP showed the highest MTC of 148.3 \pm 7.0 nм and was closely followed by the BMA modified mats with a MTC of 138.7 \pm 6.1 nm, indicating both produce a high concentration of thrombin. The unmodified PCL mats displayed a slightly lower MTC of 127.1 \pm 7.3 nm, while the control clots without a fiber mat displayed a significantly lower MTC of 81.4 \pm 7.0 nm. These values confirm that BCCP and BMA are improving the strength and stability of the fibrin clots due to increased thrombin levels when compared to controls. The AA modified mats show the lowest MTC value of 61.7 \pm 5.5 nm. These results suggest that hydrophobicity of the surface is a major driving factor in blood clot development.

2.3.3. Fibrin Clot Analysis

Clots were analyzed by scanning electron microscopy (SEM) to determine dimensions of the fibrin strands. Clots were imaged at the nanofiber/clot interface, the top of clots, and at a clot cross-section (**Figure 6**). Diameters of the fibrin strands were measured at 50 points per sample via ImageJ software and averaged (**Figure 7**). Thicker fibrin strands result in stronger clots that are more resistant to fibrinolysis. [37,39] The BCCP modified nanofiber mats displayed the largest fibrin strand diameter of 174.8 \pm 33.4 nm, which is larger than the BMA mats with the next biggest diameter of 143.5 \pm 38.1 nm. Unmodified PCL mats exhibit a diameter with no statistically significant difference from BMA of 139.7 \pm 33.7 nm. Acrylic acid and clots without fiber mats have even lower diameters of 111.5 \pm 36.6 and 99.1 \pm 33.4 nm, respectively. The clots formed from BCCP and BMA also appear to have the densest fibrin networks.

2.3.4. Discussion

PRT, MTC, and fibrin dimension model different attributes of the strength and stability of blood clots. As summarized in Table S1,

16165195, Downloaded from https://onlinelbrary.wiley.com/doi/10.1002/mabi.202200292 by University Of California, Wiley Online Library on [13/10/2022]. See the Terms and Conditions (https://onlinelbbrary.wiley.com/terms-and-conditions) on Wiley Online Library for rules of use; OA articles are governed by the applicable Creative Commons Licenses

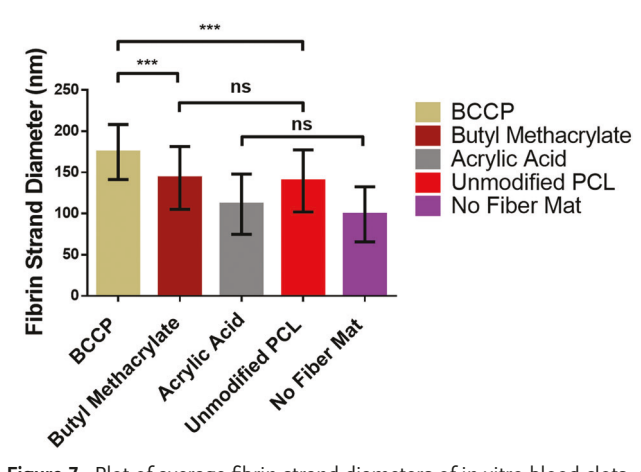


Figure 7. Plot of average fibrin strand diameters of in vitro blood clots. n = 50; *** $p \le 0.001$.

Supporting Information, BCCP and BMA mats are consistently the top performing nanofiber mats with the lowest PRT and highest MTC while BCCP produces nanofibers with the largest fibrin diameters, outperforming BMA. BMA values are statistically equivalent to those of BCCP in PRT (191.4 \pm 4.2 s vs 183.5 \pm 9.2 s) and MTC (138.7 \pm 6.3 vs 148.3 \pm 7.1 nm), while the values of fibrin strand diameter show more distinct differences (143.5 \pm 38.1 vs 174.8 \pm 33.4 nm). This indicates that the addition of acrylic acid into the polymer chain in BCCP has a more significant impact on the physical dimensions of the material while the butyl methacrylate is more responsible for improving thrombin generation, which in turn speeds up clot formation. In all experiments, AA modified mats had a significantly lower performance than the BCCP and BMA mats, as well as the unmodified PCL. AA mats also performed worse than controls without a mat with respect to PRT and MTC, while extremely close in fibrin strand diameter. Hydrophobicity of the material appears to play a major role regarding clotting effectiveness, as the AA modified mats are significantly more hydrophilic than any other sample.

3. Conclusions

This work demonstrated the successful fabrication and in vitro demonstration of blood clot enhancing, nonwoven PCL nanofiber mats via a high-throughput melt coextrusion process followed by subsequent SI-ATRP. We demonstrated that the BCCP modified mats were the most effective at accelerating time to clot, produced the most thrombin, and gave the thickest and most dense fibrin strands. Future work will entail the fabrication of multifunctional materials that combine this work with our previous antibacterial mats, along with other biomedically relevant uses such as antiviral and antifungal properties.

4. Experimental Section

Materials: CAPA 6800 PCL-80 kDa was purchased from The Perstorp Group. POLYOX N80-200 kDa and POLYOX N10-100 kDa PEO were purchased from Dow Chemical. Triethylamine (TEA) was purchased from VWR Life Science. Tris(2-dimethylaminoethyl)amine (Me₆TREN) and 1-bromohexane were purchased from Alfa Aesar. Copper (I)

bromide, α -bromoisobutyryl bromide, acrylic acid, calcium chloride, butyl methacrylate, HEPES, 25% glutaraldehyde solution in H₂O, L-A-phosphatidylcholine type XVI-E, L-A-phosphatidylserine, and bovine serum albumin (BSA) were purchased from MilliporeSigma. Sodium chloride, dimethylsulfoxide (DMSO), sodium phosphate monobasic monohydrate, and sodium phosphate dibasic heptahydrate were purchased from Fisher Chemical. Platelet poor plasma was purchased from Technoclone. Phosphate buffered saline (PBS) pH 7.4 1× was purchased from Gibco. Recombinant tissue factor (rTF) was purchased from BioLegend. Human α -thrombin was purchased from Haematologic Technologies. Ethyl alcohol, anhydrous was purchased from Electron Microscopy Sciences.

Instrumentation and Equipment: A Haake Rheodrive 5000 twin-screw extruder was used to compound PEO. A custom, two-component melt coextrusion system with a series of vertical and horizontal multipliers was used to fabricate composite tapes. Nanofibers were subjected to a SereneLife SLPRWAS26 Compact Pressure Washer (maximum pressure 1500 psi, 3 mm length by 11 mm width) to remove excess PEO and entangle nanofibers into mats. An Anytime Tools sharp 1/4" hollow punch was used to stamp nonwoven nanofiber mats into a circular shape. An Omnicure Model S1500 standard filter 320-500 nm UV light source system was used for photochemistry. A FEI Apreo LoVac FESEM was used to obtain electron micrographs. A ramé hart Model 200 goniometer was used to obtain water contact angle measurements. A Kratos Analytical AXIS Supra surface analysis instrument was used for X-ray photoelectron spectroscopy data. A Tecan Infinite M PLEX Monochromator was used to obtain fluorescence data. A Tousimis Autosamdri-815, Series A Automatic Critical Point Drier was used to dry prepared blood clots.

Melt Coextrusion of Compound Tapes: 200 and 100 kDa PEO were first mixed in a 30%/70% w/w% ratio (to achieve a rheological match to PCL at extrusion temperatures)[16] and dried for 48 h at 40 °C. The PEO was then compounded in a twin-screw extruder at 140 °C followed by pelletization.^[20] PCL and the compounded PEO pellets were then dried for 48 h at 40 °C before being coextruded at 180 °C to provide PCL nanofibers embedded in a PEO matrix. The extrusion line was comprised of 16 vertical and 4 horizontal multipliers. Between the horizontal and vertical multipliers, the extrudate was encased in a 33% by volume PEO skin layer. Completed compound tapes exited the system through a "3" tape die and were collected on a chill roll at room temperature that rotated at 15 rpm.^[30]

Removal of PEO and Preparation of PCL Mats: Composite tapes were secured inside of a beaker of stirring water for 6 h with the water being changed hourly. The tapes were then left overnight in a 70% MeOH: 30% $\rm H_2O$ solution to remove the PEO, revealing PCL fibers. Fibers were then attached to a fiberglass plate in a single layer and covered with a wire mesh to be washed with a pressure washer, varying the spray size. This high-pressure wash served two purposes: 1) to remove any remaining PEO and 2) to entangle the nanofibers to form nonwoven mats. Nonwoven mats were then dried in a desiccator overnight and 6 mm circular patches were punched out of them with a hollow punching apparatus to be used for further preparation and experimentation.

Nanofiber Functionalization with Photochemistry: Nonwoven mats (6 mm diameter, \approx 4.5 mg) were placed into a 10 mg mL⁻¹ solution of a benzophenone-ATRP initiator in MeOH, whose synthesis was previously described. Saturated nonwoven mats are placed in a vacuum desiccator and dried overnight, then subjected to a broadband UV lamp (320–500 nm) with an intensity of 548 mW cm⁻² for 35 min per side. The mats were then washed three times with methanol and dried again overnight in a vacuum desiccator. Successful functionalization was confirmed with X-ray photoelectron spectroscopy (XPS) and water contact angle (WCA).

Grafting-From ATRP: Monomer (2.13 mmol) (e.g. blood clotting copolymer utilizes 65 mol% acrylic acid and 35 mol% butyl methacrylate), Me₆TREN (7.4 mg, 0.043 mmol), dimethylformamide (2 mL), and 21 initiator-modified nonwoven mats were added to a three-neck round bottom flash and bubbled with N₂ gas for 50 min. Cu(I)Br (3.1 mg, 0.021 mmol) was then added quickly under positive N₂ pressure. The polymerization was left overnight at room temperature. The following morning, mats were removed and washed three times with MeOH then dried in a vacuum desiccator. Successful functionalization was confirmed with XPS and WCA.

Plasma Recalcification Time: Nanofiber mats (6 mm diameter circles) were placed in individual wells of a tissue culture treated 96 well plate that was first warmed in a 37 °C incubator for 5 min. 100 μL of 0.025 м CaCl₂ and 100 µL of reconstituted platelet-poor plasma (PPP) were added to the wells, quickly mixed with a micropipette, then placed in a 37 °C hot water bath for the duration of the experiment. Gelation was determined when the plasma solution became visibly cloudy and stiff. Triplicate data points were obtained; however, each sample was incubated individually to allow accurate observations and measurements. [46]

Thrombin Generation Assay: Sample nonwoven mats were placed in the wells of a black, flat-bottom 96 well plate (five replicates per sample). 1 μL of a 1 mm fluorogenic substrate (1 mm Z-Gly-Gly-Arg-AMC.HCL, 15 mм CaCl₂ in HNa buffer [25 mм HEPES and 175 mм NaCl at pH 7.35], containing 2% by volume DMSO and 0.4% by volume BSA) with 15 mm CaCl₂, 20 μL phospholipid/tissue factor mixture (3.2 μм 80%/20% by mol phosphatidylcholine/phosphatidylserine with 17.9 pm rTF in HNa buffer), and 80 µL of PPP were added to the wells, mixed, and immediately placed into a plate-reader; measuring the fluorescence every minute for 45 min. A standard curve was generated by replacing the PPP with various thrombin dilutions without the presence of the sample mats. Maximum thrombin concentrations were calculated by comparing the slopes generated from the TGA to the standard curves.[52]

Fibrin Clot Architecture Analysis: Clots were prepared as described in Plasma Recalcification Time Section, but were left for 2 h to allow the coagulation process to complete. Clots were washed for 30 min three times with PBS (pH 7.4). Clots were fixed with glutaraldehyde in a phosphate buffer prepared with 68.4% by volume of 1 M Na₂HPO₄ and 31.6% by volume of 0.1 M NaH₂PO₄, combined and diluted to give a 2% glutaraldehyde solution in 0.1~M of the combined phosphate buffer. The clots were dehydrated in absolute ethanol of varying grades (50%, 75%, and 100%) for 1 h each, then dried in a CO2 critical point drier. Following drying, the clots were submerged in liquid nitrogen and broken in half using a pair of tweezers. The prepared clots were sputter coated with gold and imaged via SEM at various points including the clot/nanofiber interface, a top view of the clots, and the clot cross-section.[43]

Statistical Analysis: Reported results are the mean with standard deviation. Unpaired t-tests were performed on plasma recalcification time, maximum thrombin concentration, and fibrin dimension analysis data. Results were considered significant if p < 0.05.

Supporting Information

Supporting Information is available from the Wiley Online Library or from the author.

Acknowledgements

The authors gratefully acknowledge the NSF Partnerships for International Research and Education (PIRE) (OISE 1844463) for their financial support. The Baer Group (Dr. Xinting Wang and Dr. Cong Zhang) is thanked for providing access and assistance with the melt coextrusion equipment. Dr. Erik Price is also acknowledged for his assistance with preparations for the melt coextrusion process. The Maia Group (Dr. Dana Klein) is thanked for providing access and assistance with the twin-screw extruder. The authors acknowledge the use of facilities and instrumentation supported by the National Science Foundation through the UC San Diego Materials Research Science and Engineering Center (UCSD MRSEC), grant DMR 2011924.

Conflict of Interest

Macromol. Biosci. 2022, 2200292

The authors declare no conflict of interest.

Data Availability Statement

The data that support the findings of this study are available from the corresponding author upon reasonable request.

Keywords

blood clotting, coagulation, fibrin, melt coextrusion, nanofibers, photochemistry, surface-initiated atom transfer radical polymerization

> Received: July 15, 2022 Revised: August 28, 2022 Published online:

- [1] H. J. Diao, K. Wang, H. Y. Long, M. Wang, S. Y. Chew, Adv. Healthcare Mater. 2016, 5, 529.
- [2] N. Nagiah, R. Johnson, R. Anderson, W. Elliott, W. Tan, Langmuir 2015, 31, 12993.
- [3] T. A. M. Valente, D. M. Silva, P. S. Gomes, M. H. Fernandes, J. D. Santos, V. Sencadas, ACS Appl. Mater. Interfaces 2016, 8, 3241.
- [4] A. M. Jordan, V. Viswanath, S.-E. Kim, J. K. Pokorski, L. T. J. Korley, J. Mater. Chem. B 2016, 4, 5958.
- [5] J. D. Hochberg, D. M. Wirth, G. Spiaggia, P. Shah, B. Rothen-Rutishauser, A. Petri-Fink, J. K. Pokorski, ACS Appl. Polym. Mater. 2022. 4. 260.
- [6] S. Agarwal, J. H. Wendorff, A. Greiner, Polymer 2008, 49, 5603.
- [7] L. A. Smith Callahan, S. Xie, I. A. Barker, J. Zheng, D. H. Reneker, A. P. Dove, M. L. Becker, Biomaterials 2013, 34, 9089.
- [8] N. Wang, K. Burugapalli, W. Song, J. Halls, F. Moussy, Y. Zheng, Y. Ma, Z. Wu, K. Li, J. Membr. Sci. 2013, 427, 207.
- [9] A. Camerlo, A.-M. Bühlmann-Popa, C. Vebert-Nardin, R. M. Rossi, G. Fortunato, I. Mater. Sci. 2014, 49, 8154.
- [10] I. Esmaeilzadeh, V. Mottaghitalab, B. Tousifar, A. Afzali, M. Lamani, Int. J. Ind. Chem. 2015, 6, 193.
- [11] M. R. Badrossamay, K. Balachandran, A. K. Capulli, H. M. Golecki, A. Agarwal, J. A. Goss, H. Kim, K. Shin, K. K. Parker, Biomaterials 2014, 35, 3188.
- [12] M. R. Badrossamay, H. A. Mcilwee, J. A. Goss, K. K. Parker, Nano Lett. 2010, 10, 2257.
- [13] F. Zuo, D. H. Tan, Z. Wang, S. Jeung, C. W. Macosko, F. S. Bates, ACS Macro Lett. 2013, 2, 301.
- [14] F. Chen, G. Hochleitner, T. Woodfield, J. Groll, P. D. Dalton, B. G. Amsden, Biomacromolecules 2016, 17, 208.
- [15] J. Wang, D. Langhe, M. Ponting, G. E. Wnek, L. T. J. Korley, E. Baer, Polymer 2014, 55, 673.
- [16] S.-E. Kim, A. M. Jordan, L. T. J. Korley, J. K. Pokorski, J. Mater. Chem. B 2017, 5, 4499.
- [17] S.-E. Kim, J. Wang, A. M. Jordan, L. T. J. Korley, E. Baer, J. K. Pokorski, ACS Macro Lett. 2014, 3, 585.
- [18] J. Wang, M. Ponting, C. Zhang, A. Olah, E. Baer, J. Membr. Sci. 2017, 526, 229.
- [19] S.-E. Kim, J. D. Wallat, E. C. Harker, A. A. Advincula, J. K. Pokorski, Polym. Chem. 2015, 6, 5683.
- [20] S.-E. Kim, E. C. Harker, A. C. De Leon, R. C. Advincula, J. K. Pokorski, Biomacromolecules 2015, 16, 860.
- [21] I. C. Ng, P. Pawijit, J. Tan, H. Yu, in Encyclopedia of Biomedical Engineering (Ed: R. Narayan), Elsevier, New York 2019, pp. 225-236.
- [22] M. S. Cortizo, M. S. Molinuevo, A. M. Cortizo, J. Tissue Eng. Regener. Med. 2008, 2, 33.
- [23] L. S. Nair, C. T. Laurencin, Prog. Polym. Sci. 2007, 32, 762.
- [24] P. Gunatillake, R. Mayadunne, R. Adhikari, Biotechnology Annual Review, Vol. 12, Elsevier, New York 2006, pp. 301-347.
- [25] B. Dhandayuthapani, Y. Yoshida, T. Maekawa, D. S. Kumar, Int. J. Polym. Sci. 2011, 2011, 290602.
- [26] A.-D. Bendrea, L. Cianga, G.-L. Ailiesei, E.-L. Ursu, D. G. Colak, I. Cianga, Polymers 2021, 13, 2720.
- [27] H. Sun, S. Önneby, Polym. Int. 2006, 55, 1336.
- [28] Y. Zhu, C. Gao, X. Liu, J. Shen, Biomacromolecules 2002, 3, 1312.

www.advancedsciencenews.com

Eioscience
www.mbs-journal.de

- [29] C. Kósa, M. Sedlačík, A. Fiedlerová, Š. Chmela, K. Borská, J. Mosnáček, Eur. Polym. J. 2015, 68, 601.
- [30] S.-E. Kim, C. Zhang, A. A. Advincula, E. Baer, J. K. Pokorski, ACS Appl. Mater. Interfaces 2016, 8, 8928.
- [31] J. W. Cannon, N. Engl. J. Med. 2018, 378, 370.
- [32] R. Lozano, M. Naghavi, K. Foreman, S. Lim, K. Shibuya, V. Aboyans, J. Abraham, T. Adair, R. Aggarwal, S. Y. Ahn, M. A. AlMazroa, M. Alvarado, H. R. Anderson, L. M. Anderson, K. G. Andrews, C. Atkinson, L. M. Baddour, S. Barker-Collo, D. H. Bartels, M. L. Bell, E. J. Benjamin, D. Bennett, K. Bhalla, B. Bikbov, A. B. Abdulhak, G. Birbeck, F. Blyth, I. Bolliger, S. Boufous, C. Bucello, et al., Lancet 2012, 380, 2095.
- [33] N. Okumura, F. Terasawa, A. Haneishi, N. Fujihara, M. Hirota-Kawadobora, K. Yamauchi, H. Ota, S. T. Lord, J. Thromb. Haemostasis 2007, 5, 2352
- [34] A. Z. Budzynski, S. A. Olexa, B. V. Pandya, Ann. N. Y. Acad. Sci. 1983, 408, 301.
- [35] S. T. Lord, Arterioscler., Thromb., Vasc. Biol. 2011, 31, 494.
- [36] G. Spraggon, S. J. Everse, R. F. Doolittle, Nature 1997, 389, 455.
- [37] B. Blomblckl, K. Carlsson, K. Fatah, B. Hesse, *Thromb. Res.* 1994, 75, 18
- [38] Z. Yang, I. Mochalkin, R. F. Doolittle, Proc. Natl. Acad. Sci. USA 2000, 97, 14156.
- [39] S. Kattula, J. R. Byrnes, A. S. Wolberg, Arterioscler., Thromb., Vasc. Biol. 2017, 37, e13.

- [40] S. A. Smith, R. J. Travers, J. H. Morrissey, Crit. Rev. Biochem. Mol. Biol. 2015, 50, 326.
- [41] H. L. Nossel, Blood 1967, 29, 331.
- [42] C. Sperling, M. Fischer, M. F. Maitz, C. Werner, Biomaterials 2009, 30, 4447.
- [43] H. T. Shiu, B. Goss, C. Lutton, R. Crawford, Y. Xiao, J. Mater. Chem. B 2014, 2, 3009.
- [44] M. K. Rausch, S. H. Parekh, B. Dortdivanlioglu, A. M. Rosales, Prog. Biomed. Eng. 2021, 3, 042006.
- [45] G. Arul, D. Bowley, S. Dirusso, J. R. Army Med. Corps 2012, 158, 331.
- [46] N. Ayres, D. J. Holt, C. F. Jones, L. E. Corum, D. W. Grainger, J. Polym. Sci., Part A: Polym. Chem. 2008, 46, 7713.
- [47] J. R. Lancaster, R. Smilowitz, N. J. Turro, J. T. Koberstein, *Photochem. Photobiol.* 2014, 90, 394.
- [48] R. Förch, H. Schönherr, A. T. A. Jenkins, Surface Design: Applications in Bioscience and Nanotechnology, John Wiley & Sons, Hoboken, NJ 2009.
- [49] J. Mellanby, C. L. G. Pratt, Proc. R. Soc. B 1940, 128, 201.
- [50] K. G. Mann, M. F. Whelihan, S. Butenas, T. Orfeo, J. Thromb. Haemostasis 2007, 5, 2055.
- [51] E. A. Ryan, L. F. Mockros, J. W. Weisel, L. Lorand, *Biophys. J.* 1999, 77, 2813.
- [52] G. L. Salvagno, E. Berntorp, in *Hemostasis and Thrombosis* (Eds: E. J. Favaloro, G. Lippi), Methods in Molecular Biology, Vol. 1646, Springer, New York 2017, pp. 515–522.